

Polarization observables in the semiexclusive photoinduced three-body breakup of ^3He .

R. Skibiński¹, J. Golak¹, H. Witała¹, W. Glöckle², A. Nogga³, H. Kamada⁴

¹*M. Smoluchowski Institute of Physics, Jagiellonian University, PL-30059 Kraków, Poland*

²*Institut für Theoretische Physik II, Ruhr-Universität Bochum, D-44780 Bochum, Germany*

³*Forschungszentrum Jülich, Institut für Kernphysik (Theorie), D-52425 Jülich, Germany*

⁴*Department of Physics, Faculty of Engineering, Kyushu Institute of Technology, 1-1 Sensuicho, Tobata, Kitakyushu 804-8550, Japan*

(September 9, 2018)

Abstract

The photon and ^3He analyzing powers as well as spin correlation coefficients in the semiexclusive three-body photodisintegration of ^3He are investigated for incoming photon laboratory energies $E_\gamma=12, 40$ and 120 MeV. The nuclear states are obtained by solving three-body Faddeev equations with the AV18 nucleon-nucleon potential alone or supplemented with the UrbanaIX three-nucleon force. Explicit π - and ρ -meson exchange currents are taken into account, but we also compare to other models of the electromagnetic current. In some kinematical conditions we have found strong effects of the three-nucleon force for the ^3He analyzing power and spin correlation coefficients, as well strong sensitivities to the choice of the currents. This set of predictions should be a useful guidance for the planning of measurements. In addition, we compare our results for two-body ^3He breakup induced by polarized photons with a few existing data.

21.45.+v, 24.70.+s, 25.10.+s, 25.20.-x

I. INTRODUCTION

The study of polarization phenomena is a natural extension of investigation of unpolarized processes. It provides additional information on details of the underlying nuclear Hamiltonian not available in unpolarized reactions. In nucleon-nucleon (NN) systems the polarized processes provide a necessary data set to construct the NN potentials [1]. The investigation of nucleon-deuteron (Nd) elastic scattering and the deuteron breakup reaction with polarized incoming nuclei or polarization of the outgoing particles measured is indispensable to learn about properties of the three-nucleon (3N) forces. Nowadays spin observables in Nd elastic scattering where the initial deuteron and/or nucleon is polarized and also the polarization of the final particles is measured, are available and can be compared with rigorous theoretical predictions [2–5]. Also for deuteron breakup such studies were performed, both experimentally [6–8] as well as theoretically [9,10]. Altogether, this allowed to test the current models of the nuclear Hamiltonian.

In addition to the strong forces, the electromagnetic processes contain new dynamical ingredients due to the interaction between real or virtual photons with the currents of nuclei. It was found that in such processes contributions to the nuclear current due to meson exchanges play an important role. Studies of polarization observables in photo- and electro-induced processes on the deuteron [11], as well as in the Nd radiative capture [12–16] can be used to determine the structure of nuclear currents. The combination of strong and electromagnetic interactions is a demanding test for theoretical models. The results up to now show an overall good agreement of theoretical predictions with the data, however there is still room for improvement [17]. Recently an important progress is observed in experimental investigations of processes with polarized photons. The high-intensity sources of highly polarized photon beams obtained by the Compton backscattering give hope for future precise data [18]. The analysis of the first measurement of the ${}^3\text{He}$ breakup using polarized photons at low energies is in progress and was reported recently in [19].

In this paper we would like to present the results of theoretical investigations of spin observables in kinematically incomplete $\vec{\gamma}({}^3\vec{H}e, N)NN$ processes in which the incoming photon and/or the ${}^3\text{He}$ nucleus are polarized. This study is done for three photon laboratory energies $E_\gamma=12, 40$ and 120 MeV. For each photon energy, the energy spectrum of the detected outgoing nucleon at different angles has been calculated. We restrict ourselves to photon energies below the pion production threshold and have chosen the above energies as examples of low, intermediate and high photon energies. It was shown in [20] that for those energies one can expect different manifestations of the action of the 3N force in two-body photodisintegration of ${}^3\text{He}$. While at low energies the inclusion of the three-nucleon forces decreases the cross section, at higher energies 3N forces act in the opposite direction. At intermediate energies the influence of 3N forces on the two and three-body breakup cross sections is negligible. As will be shown in section III for several spin observables the influence of 3N forces is visible in the semiexclusive spectrum of the outgoing nucleon also at intermediate energies of the incoming photon. The presented results should be a useful guide for future experiments. Up to now, to the best of our knowledge, no such predictions have been published.

In section II we shortly describe the theoretical formalism underlying our calculations and give definitions for the studied spin observables. In section III we present our predictions

for three-body breakup. In addition we turn into two-body ${}^3\text{He}$ breakup and compare our results to a few existing data. We summarize in section IV.

II. THEORETICAL FRAMEWORK

The theoretical framework we use is described in detail in Refs. [13,17,20,21]. For the convenience of the reader we briefly summarize the most important steps. The basic nuclear matrix element $N_{m_i,\tau,m}^{\text{3N}}$ is expressed through the state $|\tilde{U}_\tau^m\rangle$ which fulfills the Faddeev-like equation

$$|\tilde{U}_\tau^m\rangle = (1+P)j_\tau(\vec{Q})|\Psi_{{}^3\text{He}}^m\rangle + \left(tG_0P + \frac{1}{2}(1+P)V_4^{(1)}G_0(tG_0+1)P\right)|\tilde{U}_\tau^m\rangle. \quad (1)$$

Here $j_\tau(\vec{Q})$ is a spherical τ -component of the ${}^3\text{He}$ electromagnetic current operator, t the NN t-matrix, G_0 the free 3N propagator and P the sum of the cyclical and anticyclical permutations of 3 particles. Further $V_4^{(1)}$ is that part of the 3NF, which is symmetrical (like the NN t -matrix) under the exchange of nucleons 2 and 3, and $|\Psi_{{}^3\text{He}}^m\rangle$ is the ${}^3\text{He}$ bound state with spin projection m . The nuclear matrix element for three-body breakup of ${}^3\text{He}$ is given via

$$N_{m_i,\tau,m}^{\text{3N}} = \frac{1}{2}\langle\Phi_0^{m_i}|(tG_0+1)P|\tilde{U}_\tau^m\rangle, \quad (2)$$

where $\langle\Phi_0^{m_i}|$ is the properly anti-symmetrized (in the two-body subsystem) state of three free nucleons with their spin projections m_i .

Given the $N_{m_i,\tau,m}^{\text{3N}}$ amplitudes, one can calculate any polarization observables. They are expressed through the nuclear matrix elements with different spin projections carried by the initial photon, the ${}^3\text{He}$ nucleus, and by the outgoing nucleons.

Choosing the z-axis to be the direction of the incoming photon and allowing for a linear photon polarization P_0^γ along the x-axis, with the polarization component $P_0^\gamma = -1$, and for the ${}^3\text{He}$ target nucleus polarization $P_0^{{}^3\text{He}}$ along the y-axis, the cross section in a kinematically incomplete reaction $\vec{\gamma}({}^3\text{He}, N)NN$, when the outgoing nucleon is detected at angles (θ, ϕ) is given by

$$\sigma_{\gamma,{}^3\text{He}}^{\text{pol}}(\theta, \phi) = \sigma_{\gamma,{}^3\text{He}}^{\text{unpol}}(\theta)[1 + P_0^\gamma \cos(2\phi) A_x^\gamma(\theta) + P_0^{{}^3\text{He}} \cos(\phi) A_y^{{}^3\text{He}}(\theta) + P_0^\gamma \cos(2\phi) P_0^{{}^3\text{He}} \cos(\phi) C_{x,y}^{{}^3\text{He}}(\theta) + P_0^\gamma \sin(2\phi) P_0^{{}^3\text{He}} \sin(\phi) C_{y,x}^{{}^3\text{He}}(\theta)]. \quad (3)$$

Here the nonvanishing spin observables are the photon ($A_x^\gamma(\theta)$) and the ${}^3\text{He}$ ($A_y^{{}^3\text{He}}(\theta)$) analyzing powers, and the spin correlation coefficients $C_{x,y}^{{}^3\text{He}}(\theta)$ and $C_{y,x}^{{}^3\text{He}}(\theta)$. They can be obtained by measuring the spectra of the outgoing nucleon using a proper combination of ϕ angles and are expressed through the nuclear matrix element $N_{m_i,\tau,m}^{\text{3N}}$ by:

$$A_x^\gamma(\theta) \equiv \frac{\sum_{m_i m} (2\Re\{N_{m_i,-1m} N_{m_i,+1m}^*\})}{\sum_{m_i m} (|N_{m_i,+1m}|^2 + |N_{m_i,-1m}|^2)}$$

$$A_y^{{}^3\text{He}}(\theta) \equiv \frac{\sum_{m_i} (-2\Im\{N_{m_i,-1-\frac{1}{2}} N_{m_i,-1+\frac{1}{2}}^*\} - 2\Im\{N_{m_i,+1-\frac{1}{2}} N_{m_i,+1+\frac{1}{2}}^*\})}{\sum_{m_i m} (|N_{m_i,+1m}|^2 + |N_{m_i,-1m}|^2)}$$

$$\begin{aligned}
C_{x,y}^{\gamma,{}^3He}(\theta) &\equiv \frac{\sum_{m_i} (-2\Im\{N_{m_i,-1-\frac{1}{2}}N_{m_i,+1\frac{1}{2}}^*\} + 2\Im\{N_{m_i,-1\frac{1}{2}}N_{m_i,+1-\frac{1}{2}}^*\})}{\sum_{m_i m} (|N_{m_i,+1m}|^2 + |N_{m_i,-1m}|^2)} \\
C_{y,x}^{\gamma,{}^3He}(\theta) &\equiv \frac{\sum_{m_i} (2\Im\{N_{m_i,-1-\frac{1}{2}}N_{m_i,+1\frac{1}{2}}^*\} + 2\Im\{N_{m_i,-1\frac{1}{2}}N_{m_i,+1-\frac{1}{2}}^*\})}{\sum_{m_i m} (|N_{m_i,+1m}|^2 + |N_{m_i,-1m}|^2)}.
\end{aligned} \tag{4}$$

III. RESULTS

We solved Eq.(1) using a momentum space partial wave decomposition and the AV18 nucleon-nucleon potential [22] alone or supplemented with the Urbana IX 3NF [23]. For both parities and the total angular momentum of the 3N system $J \leq \frac{15}{2}$ all partial waves with angular momenta in the two-body subsystem $j \leq 3$ have been used. We refer to [21] for more details on our basis, partial wave decomposition and numerics. The electromagnetic nuclear current operator was taken as the single nucleon current supplemented by the exchange currents of the π - and ρ -like nature [12].

Before presenting the polarization observables, for the sake of completeness, we would like to show the unpolarized cross section for the $\gamma({}^3He, N)NN$ reaction with the detected outgoing nucleon to be a proton (Fig. 1) or a neutron (Fig. 2). We choose the detection polar angle θ to be $\theta = 30^\circ, 60^\circ, 90^\circ, 120^\circ$ or 150° . The spectra at $\theta = 90^\circ$ were already presented in [20]. The structures seen in these spectra originate from an interplay between strong final state interactions, meson exchange currents, phase space factors and the properties of the 3N bound state wave function. For example, for the neutron spectrum at $E_\gamma = 120$ MeV and $\theta = 90^\circ$ two peaks around $E_n \approx 20$ and 70 MeV come from the final state interactions between two nucleons. The maximum around 50 MeV comes from the interplay between the two-body currents, the phase space factors and the properties of the 3He bound state wave function. As is seen in Figs. 1 and 2 that structure depends smoothly on the angle of the outgoing nucleon with the largest cross sections around $\theta = 90^\circ$. The Urbana IX 3NF effects are visible at the lower and the upper energies of the incoming photon, and are nearly negligible at the intermediate energy.

The photon analyzing power $A_x^\gamma(\theta)$ are shown in Figs. 3-4. For photon energies $E_\gamma = 12$ and 40 MeV and detecting protons this observable decreases with increasing proton energy and reaches values -1 and -0.8 at the highest proton energies, respectively. $A_x^\gamma(\theta)$ is rather insensitive to the 3NF at these photon energies. However, at $E_\gamma = 120$ MeV the 3NF effects become sizable, and they change the photon analyzing power by up to $\approx 10\%$. The strongest effects are visible at protons energies around 25-50 MeV and at lower detection angles. For the detected neutron $A_x^\gamma(\theta)$ reaches values -1 for $E_\gamma = 12$ and 40 MeV at the upper ends of the spectra. At $E_\gamma = 120$ MeV the value of the photon analyzing power is small (up to ≈ -0.2) except in of the region of maximal energies of the detected neutrons. At all investigated energies the 3NF effects are negligible when the neutron is detected.

Contrary to a rather small 3NF effects in the photon analyzing power, the 3He analyzing power $A_y^{{}^3He}(\theta)$ is sensitive to the action of 3N forces (see Figs. 5-6). This is the case especially for the two lowest photon energies and the detected neutron and at $E_\gamma = 12$ MeV and $E_\gamma = 120$ MeV when the proton is measured. For the detected neutron the largest 3NF effects of up to 15% are at $E_\gamma = 12$ MeV and they are seen in the whole neutron spectrum.

In the proton case the most interesting situation is the highest photon energy $E_\gamma = 120$ MeV, where 3NF effects of a magnitude above $\approx 20\%$ are seen nearly for all energies of the detected proton. The action of the 3NF shifts the predictions in the opposite directions for the lowest and the highest photon energy. Unfortunately in the case of the detected proton the 3NF effects occur at relatively small (below 0.1) absolute values of $A_y^{3He}(\theta)$. For the detected neutron 3NF effects occur also for $A_y^{3He}(\theta) \leq 0.12$. However, in this case 3NF effects are seen even at intermediate photon energy, at all neutron angles and in the whole energy range. The structure of the spectrum is again due to an interplay of all dynamical components in the nuclear matrix elements. The dependence of the nuclear analyzing power on the direction of the outgoing nucleon is rather smooth, but the shape of the spectra changes significantly for different photon energies.

The spin correlation coefficients $C_{x,y}^{\gamma,3He}(\theta)$ are shown in Figs. 7-8. In that case the largest 3NF effects ($\approx 15\%$) occur in the whole spectrum at $E_\gamma = 12$ MeV when the neutron is measured. Smaller 3NF effects are also visible at other photon energies, however, their magnitude depends on the detection angle. For the measured proton, 3NF effects are negligible at the two higher photon energies. The absolute values of $C_{x,y}^{\gamma,3He}(\theta)$ for the detected proton (neutron) stays below ≈ 0.25 (≈ 0.1) at $E_\gamma = 12$ MeV and ≈ 0.4 (≈ 0.25) at the two higher photon energies.

A similar picture arises for the spin correlation coefficients $C_{y,x}^{\gamma,3He}(\theta)$ (see Figs. 9-10). Here 3NF effects are also visible at higher photon energies. For $E_\gamma = 40$ MeV and the measured neutron, 3NF effects are largest around the outgoing neutron energy ≈ 16 MeV and $\theta = 60^\circ - 120^\circ$. The absolute values of $C_{y,x}^{\gamma,3He}(\theta)$ for neutron detection are below ≈ 0.1 for $E_\gamma = 12$ and 40 MeV, and approach up to ≈ 0.4 for $E_\gamma = 120$ MeV. For the measured proton $C_{y,x}^{\gamma,3He}(\theta)$ reaches 0.25, 0.5 and 0.25 for $E_\gamma = 12, 40$ and 120 MeV, respectively. In the case of the detected proton the small 3NF effects (below 10%) occur at all photon and nucleon energies and at all detection angles.

Now we would like to address the sensitivity of the spin observables to the nuclear current used. To study this, we compare the predictions for the above spin observables at the detection angle $\theta = 90^\circ$ for three different choices of the current operator: the single nucleon current (SNC) only, when the explicit two-body meson exchange currents are added to the SNC, and finally when the current operator is constructed using the Siegert theorem [12]. The Siegert approach will also include 3N currents in the electric multipoles. We should mention, however, that in our realization of the Siegert theorem [12] we keep only single nucleon operators and do not (yet) supplement the magnetic multipoles by the explicit π - and ρ - exchange currents. Also the explicit π - and ρ - currents are not fully consistent with the underlying AV18 NN force, but only with its dominant parts [24]. For a recent investigation filling that gap see [16]. Despite these defects we think that the comparison of our Siegert approach with the explicit use of the π - and ρ - currents will enable us to identify those observables, which are especially sensitive to the choice of two and possibly three-body currents.

The photon analyzing power $A_x^\gamma(\theta)$ is insensitive to such a change of the nuclear current at the lowest energy (see Fig. 11). At $E_\gamma = 40$ MeV only a slight shift of predictions is observed under inclusion of the meson exchange currents. The effects coming from the two models of exchange currents are insignificant for the neutron knockout but lead to a small spread of theoretical predictions for the proton detection. At $E_\gamma = 120$ MeV one finds a

clear difference when the two models including exchange currents are used, and when only the single nucleon current is taken into account. The difference between SNC predictions and explicit π - and ρ - currents (Siegert) results amounts up to 140% (180%) at $E_n \approx 20$ MeV, and up to 650% (880%) at $E_p \approx 17$ MeV, respectively.

For $A_y^{^3He}(\theta)$, shown in Fig. 12 the single nucleon current predictions differ from others at all photon energies. While for the detected neutron meson exchange currents play an important role at all studied energies, in the proton case they are important only at $E_\gamma = 120$ MeV. The differences between Siegert and MEC are visible at all photon energies. At $E_\gamma = 40$ MeV they reach up to $\approx 50\%$ for neutron energies around 5-10 MeV. The case of the measured proton around $E_p \leq 15$ MeV and for $E_\gamma = 120$ MeV seems to be very interesting, since the different nuclear currents lead to a different sign of $A_y^{^3He}(\theta)$ (see Fig. 12). The differences are also seen for the spin correlation coefficients $C_{x,y}^{\gamma,^3He}(\theta)$ and $C_{y,x}^{\gamma,^3He}(\theta)$, presented in Figs. 13-14. For $C_{x,y}^{\gamma,^3He}(\theta)$ and the measured neutron there are clear differences, when using Siegert approach or direct π - and ρ - currents. They amount up to $\approx 50\%$ at $E_\gamma = 40$ MeV. For both cases, the neutron or proton detection, and $E_\gamma = 12$ MeV the predictions without 3NF differ significantly, while the inclusion of the Urbana IX force leads to an agreement between both predictions. Both spin correlation coefficients are strongly influenced by the meson exchange currents. Even at $E_\gamma = 12$ MeV single nucleon current predictions differ significantly from results based on the nuclear current supplemented by exchange currents. The role of exchange currents grows with the photon energy. In the case of $C_{y,x}^{\gamma,^3He}(\theta)$, $E_\gamma = 40$ MeV and proton energies below $E_p \leq 9$ MeV, we observe different action of the exchange currents when they are included via Siegert or by the explicit π - and ρ - exchanges. It shows that this observable is very interesting to study details of the nuclear current operator and deserves experimental efforts. Thus we can state that the spin observables in the $\vec{\gamma}(^3\vec{He}, N)NN$ reaction can provide valuable information about the nuclear current operator.

Finally, we address ourselves to the $\vec{\gamma}(^3\vec{He}, p)d$ process and compare our results with the data of Ref. [25]. There the cross section asymmetry

$$\Sigma \equiv \frac{d\sigma_{\parallel} - d\sigma_{\perp}}{d\sigma_{\parallel} + d\sigma_{\perp}}, \quad (5)$$

where $d\sigma_{\parallel}$ ($d\sigma_{\perp}$) is the cross section measured parallelly (perpendicularly) to the photon polarization direction, was investigated for linearly polarized photons with energies above 90 MeV. In Fig. 15 we compare our predictions to the data of [25] at the photon energy $E_\gamma = 120$ MeV. We see that two of the three data points are in good agreement with our theory. Our prediction at the third data point is too low in comparison to data. The 3NF shifts the theory in the right direction into the two data points. Unfortunately, most of the data points taken in [25] are at photon energies above the pion production threshold where our formalism is not adequate. Nevertheless, in Fig. 16 we compare our predictions with data at $E_\gamma = 200$ MeV in order to check if our predictions at higher energies give at least a qualitative description of the data. We see that while the shape of the theoretical predictions is similar to the shape of the data, the absolute values of the predicted analyzing power are too small by a factor of 2. This probably can be traced back to the missing dynamical ingredients in our theoretical framework, which may become important at such high energies. As was the case at $E_\gamma = 120$ MeV, also at $E_\gamma = 200$ MeV the 3NF improves

the description of the data. Since our calculations are much more advanced than the one used in Ref. [25], we would like to point out, that the very good description of the data presented in [25] might be to some extent accidental.

IV. SUMMARY

We investigated all the nonvanishing spin observables in the three-body, semiexclusive ${}^3\text{He}$ photodisintegration process when the incoming photon and/or the ${}^3\text{He}$ target nucleus are polarized. We found that the dependence of those spin observables on the angle of the outgoing nucleon is rather smooth and in most cases the shape of the energy spectra slightly changes with the incoming photon energy. In the case of the $A_y^{{}^3\text{He}}(\theta)$ analyzing power and the spin correlation coefficients $C_{x,y}^{{}^3\text{He}}(\theta)$ and $C_{y,x}^{{}^3\text{He}}(\theta)$ clear effects of the 3NF are seen. Some of the observables (e.g. $C_{y,x}^{{}^3\text{He}}(\theta)$) are sensitive to the details of the many-body contributions to the nuclear current operator, which we exemplified by using the single nucleon current alone and by supplementing it either with explicit inclusion of π - and ρ -meson exchange currents or by applying the Siegert theorem.

The presented results show that the polarization observables for ${}^3\text{He}$ photodisintegration, even in the relatively simple semiexclusive experiments, could provide valuable data to test the nuclear forces and/or the reaction mechanism. These observables should be studied experimentally. On the other hand, there are observables (e.g. $A_x^\gamma(\theta)$ at $E_\gamma=12$ MeV) which are insensitive to the chosen current operator model and to the inclusion of the 3N force. Such observables are natural candidates to test the most simple dynamical ingredients.

ACKNOWLEDGMENTS

This work was supported by the Polish Committee for Scientific Research under Grant No. 2P03B0825 and NATO Grant No. PST.CLG.978943. W.G. would like to thank the Polish-German Academical Society. The numerical calculations have been performed on the Cray SV1 and IBM Regatta p690+ of the NIC in Jülich, Germany.

REFERENCES

- [1] V. Stoks, R. Klomp, M. Rentmeester, and J. de Swart, Phys. Rev. **C48**, 792 (1993).
- [2] H. Witała, W. Glöckle, J. Golak, A. Nogga, H. Kamada, R. Skibiński, and J. Kuroś-Żołnierczuk, Phys. Rev. **C63**, 024007 (2001).
- [3] H. Witała, J. Golak, R. Skibiński, C.R. Howell, and W. Tornow, Phys. Rev. **C67** 064002 (2003).
- [4] E. Epelbaum, A. Nogga, W. Glöckle, H. Kamada, Ulf-G. Meißner, and H. Witała, Phys. Rev. **C66** 064001 (2002).
- [5] A. Kievsky, S. Rosati, and M. Viviani, Phys. Rev. **C64**, 041001R (2001).
- [6] M. Allet et al., Phys. Rev. **C50**, 602 (1994).
- [7] L.M. Qin et al., Nucl. Phys. **A587**, 252 (1995).
- [8] E. Stephan et al., in *Proceedings of The 19th European Conference on Few-Body Problems in Physics*, edited by N.Kalantar-Nayestanaki, R.G.E. Timmermans, and B.L.G. Bakker, AIP Conf. Proc. 768 (AIP, Melville, NY, 2005), p.73.
- [9] J. Kuroś-Żołnierczuk, H. Witała, J. Golak, H. Kamada, A. Nogga, R. Skibiński, and W. Glöckle, Phys. Rev. C **66**, 024003 (2002).
- [10] J. Kuroś-Żołnierczuk, H. Witała, J. Golak, H. Kamada, A. Nogga, R. Skibiński, and W. Glöckle, Phys. Rev. C **66**, 024004 (2002).
- [11] H. Arenhövel, W. Leidemann, and E.L. Tomusiak, nucl-th/0407053, and references therein.
- [12] J. Golak et al., Phys. Rev. **C62**, 054005 (2000).
- [13] R. Skibiński, J. Golak, H. Kamada, H. Witała, W. Glöckle, and A. Nogga, Phys. Rev. **C67**, 054001 (2003).
- [14] M. Viviani, A. Kievsky, L.E. Marcucci, S. Rosati, and R. Schiavilla, Phys. Rev. **C61**, 064001 (2000).
- [15] A. Deltuva, L.P.Yuan, J. Adam Jr, A.C. Fonseca, and P.U. Sauer, Phys. Rev. **C69**, 034004 (2004).
- [16] L. E. Marcucci, M. Viviani, R. Schiavilla, A. Kievsky, and S. Rosati, nucl-th/0502048, to be published in PRC
- [17] J. Golak, R. Skibiński, H. Witala, W. Glöckle, A. Nogga, and H. Kamada, nucl-th/0505072.
- [18] W. Tornow et al., Phys. Lett. **B574**, 8 (2003).
- [19] W. Tornow et al., in *Proceedings of The 19th European Conference on Few-Body Problems in Physics*, edited by N.Kalantar-Nayestanaki, R.G.E. Timmermans, and B.L.G. Bakker, AIP Conf. Proceed. 768 (AIP, Melville, NY, 2005), p.138.
- [20] R. Skibiński, J. Golak, H. Kamada, H. Witała, W. Glöckle, and A. Nogga, Phys. Rev. **C67**, 054002 (2003).
- [21] W. Glöckle, H. Witała, D. Hüber, H. Kamada, and J. Golak, Phys. Rep. **274**, 107 (1996).
- [22] R. B. Wiringa, V.G.J. Stoks, and R. Schiavilla, Phys. Rev. **C51**, (1995) 38.
- [23] B. S. Pudliner, V. R. Pandharipande, J. Carlson, Steven C. Pieper, and R. B. Wiringa, Phys. Rev. **C56**, 1720 (1997).
- [24] J. Carlson and R. Schiavilla, Rev. Mod. Phys. **70**, 743 (1998).
- [25] A.A.Belyaev, V.B.Ganenko at al., Sov. J.Nucl.Phys. **44**, 181 (1986).

FIGURES

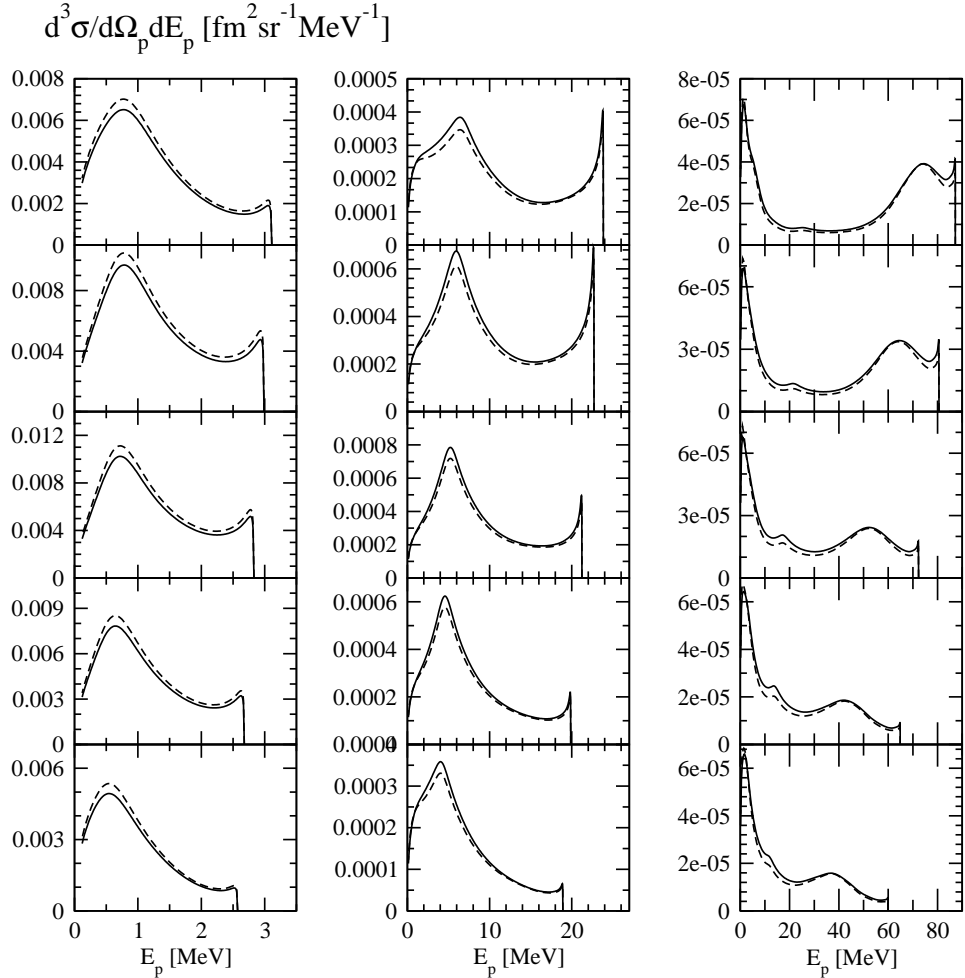


FIG. 1. The differential cross section $d\sigma^3/d\Omega_p dE_p$ for $E_\gamma = 12$ MeV (the first column), 40 MeV (the second column) and 120 MeV (the third column) at different outgoing proton angles. The first, second, third, forth and fifth row correspond to the detection angle $\theta_p = 30^\circ, 60^\circ, 90^\circ, 120^\circ$ and 150° , respectively. The dashed (solid) curve represents the AV18 (AV18+Urbana IX) predictions.

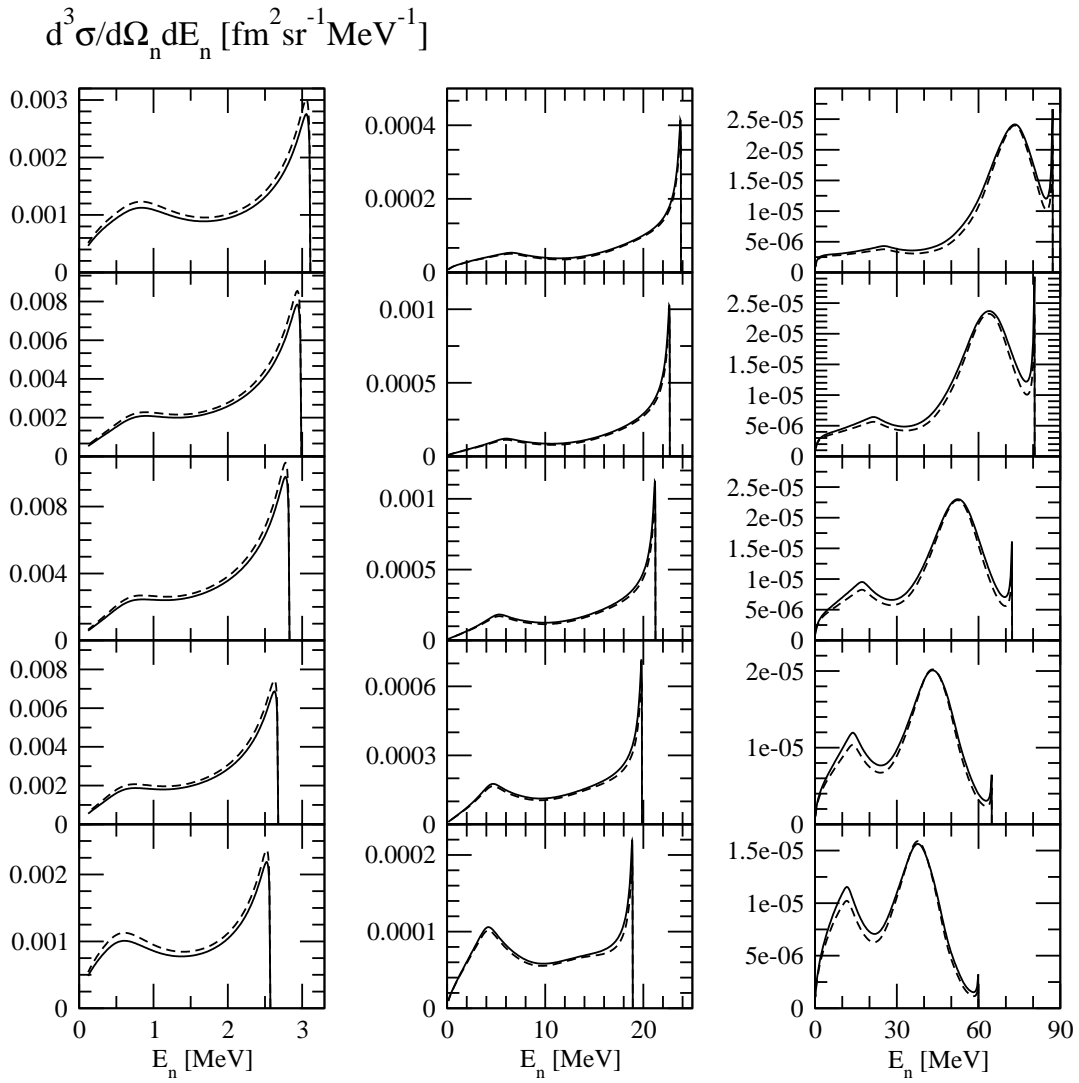


FIG. 2. The same as in Fig. 1 but for the neutron knockout.

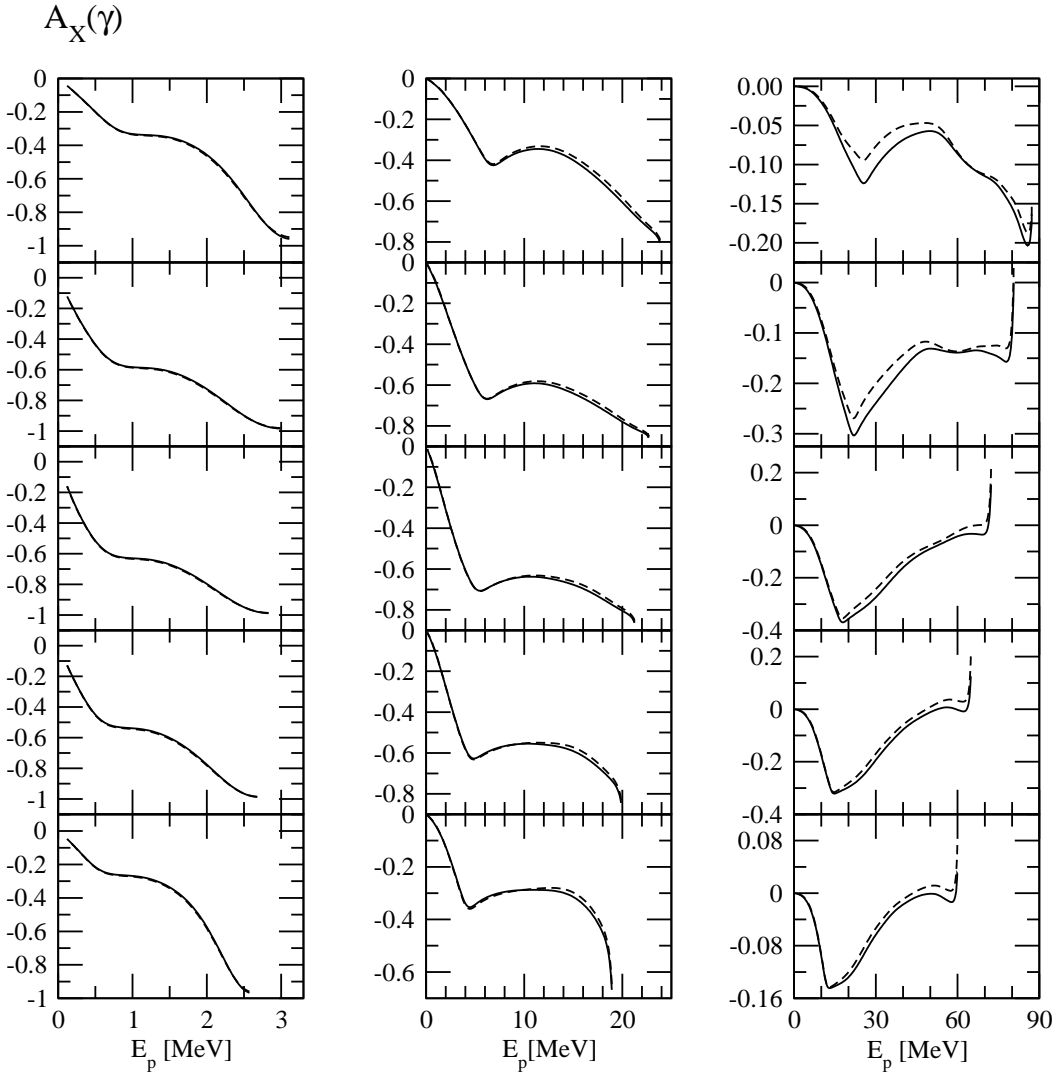


FIG. 3. The photon analyzing power $A_x^{\gamma}(\theta)$ for the proton emission. The incoming photon energies, angles and curves are the same as in Fig 1.

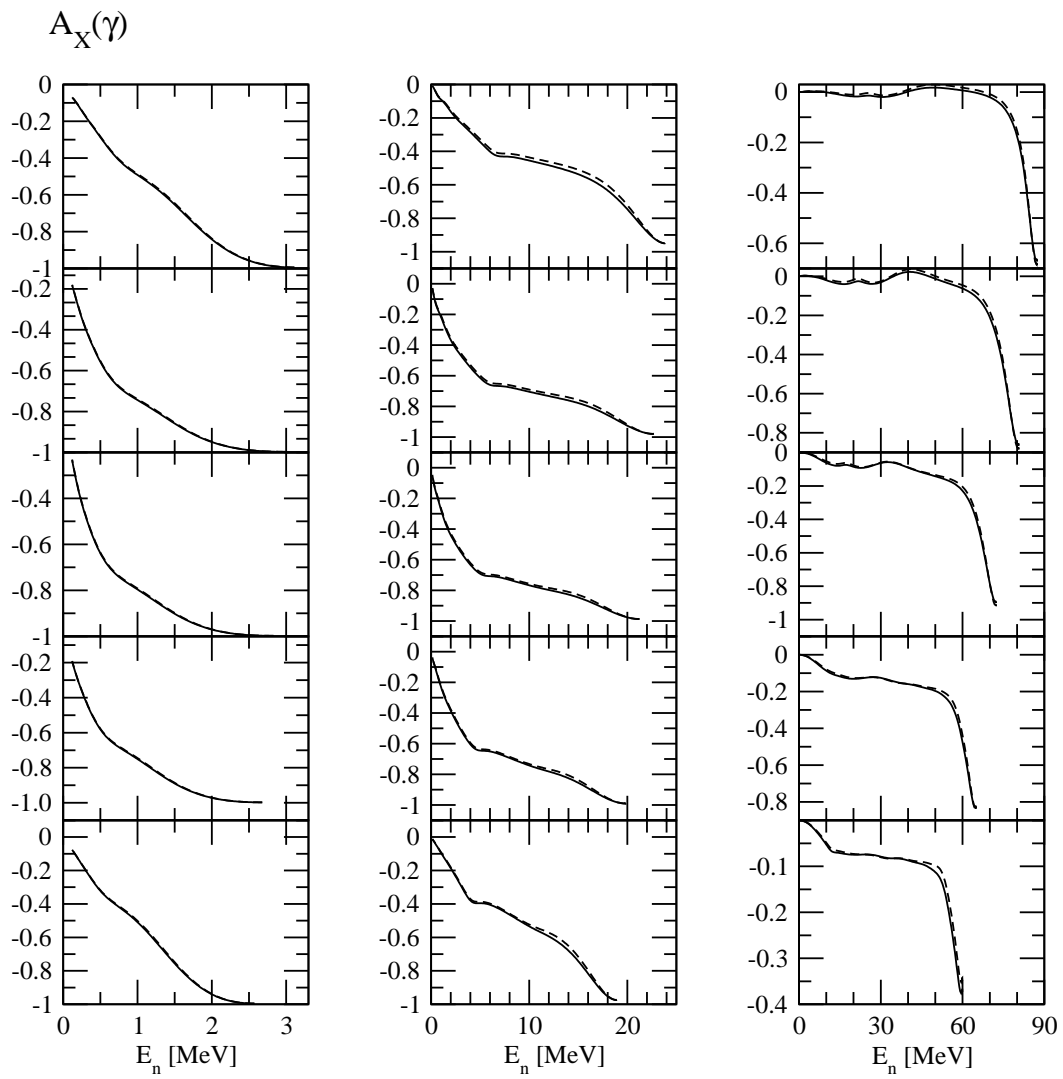


FIG. 4. The same as in Fig. 3 but for the neutron knockout.

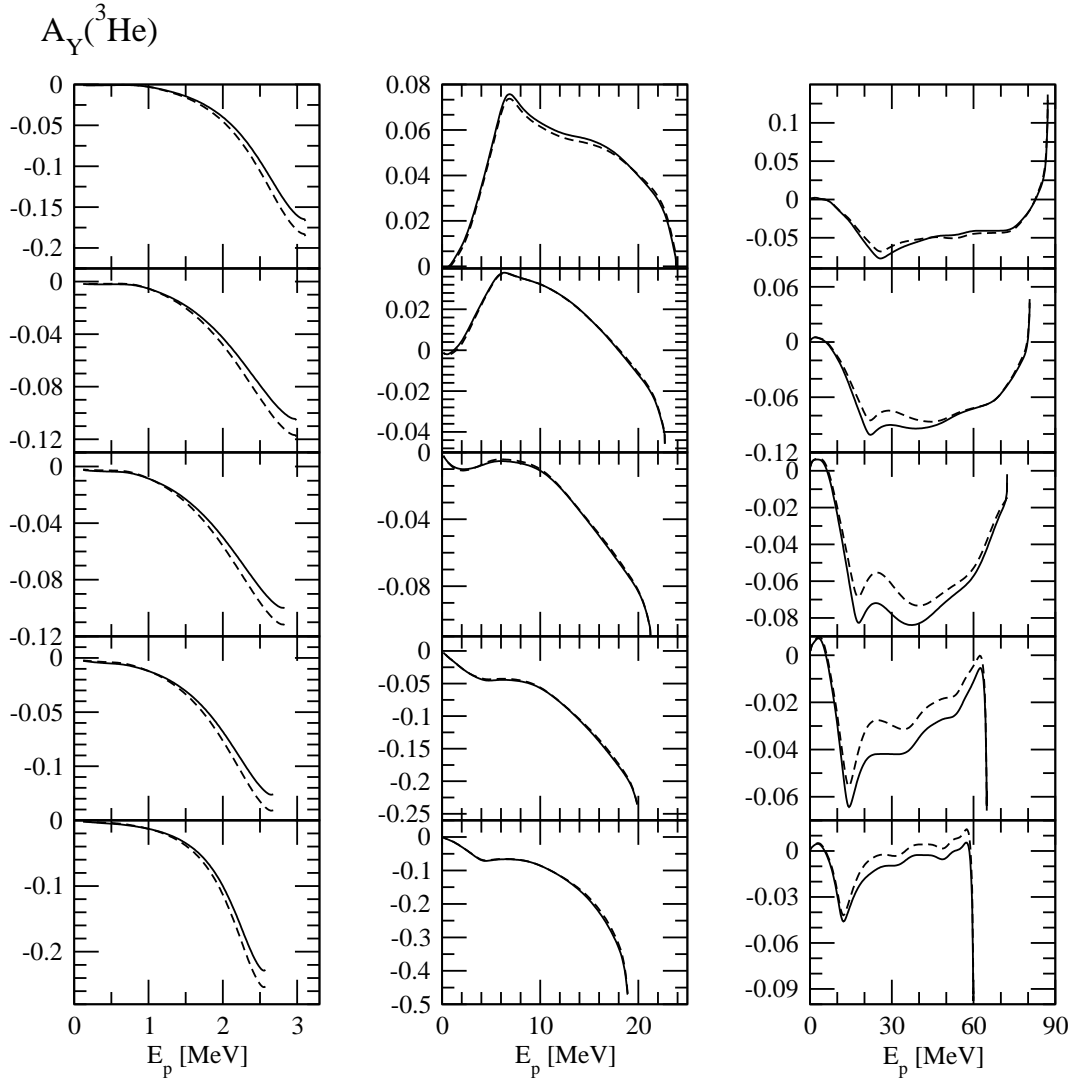


FIG. 5. The ^3He analyzing power $A_y^{^3He}(\theta)$ for the proton emission. The photon energies, angles and the curves are as in Fig 1.

$A_Y(^3\text{He})$

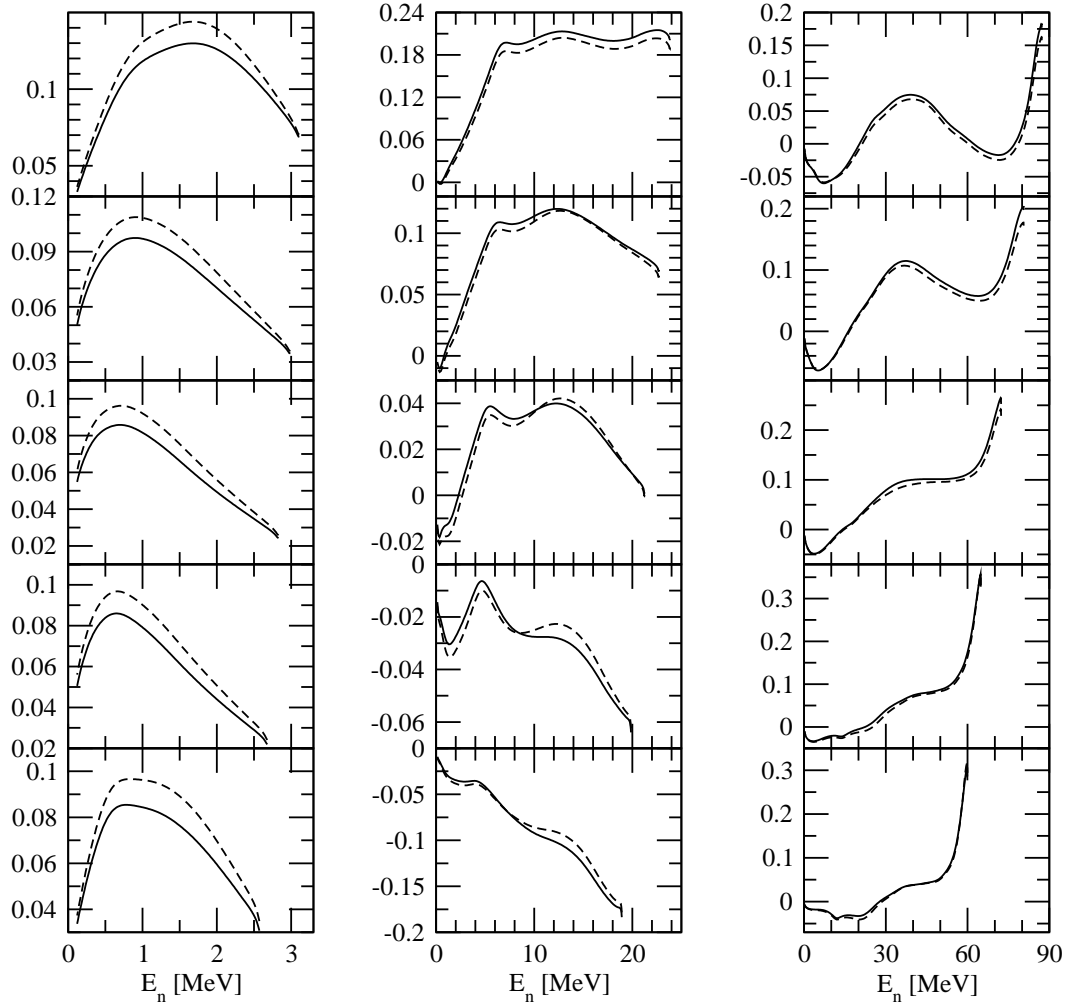


FIG. 6. The same as in Fig. 5 but for the neutron knockout.

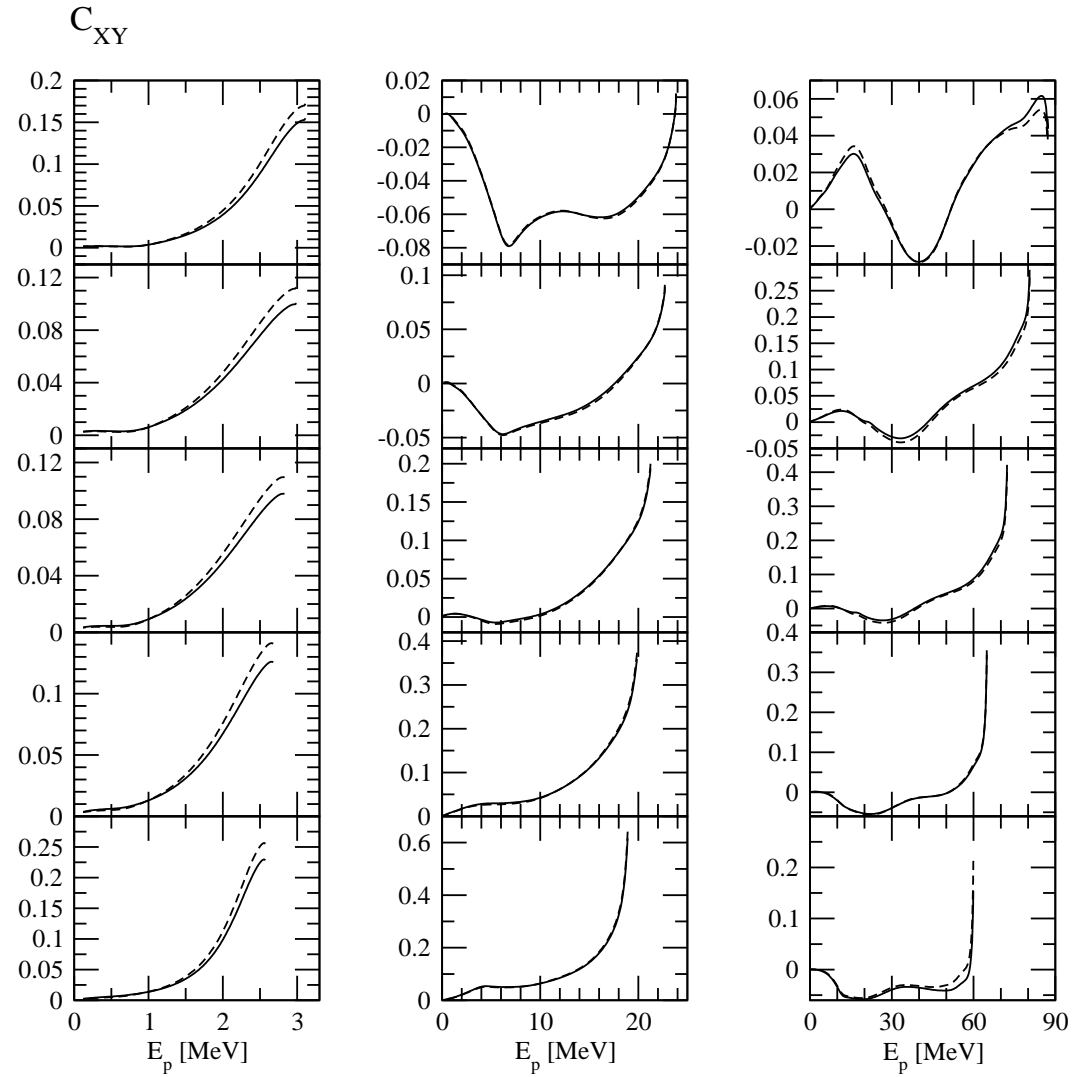


FIG. 7. The spin correlation coefficients $C_{x,y}^{\gamma,{}^3He}(\theta)$ for the proton emission. The energies, angles and the curves are as in Fig 1.

C_{XY}

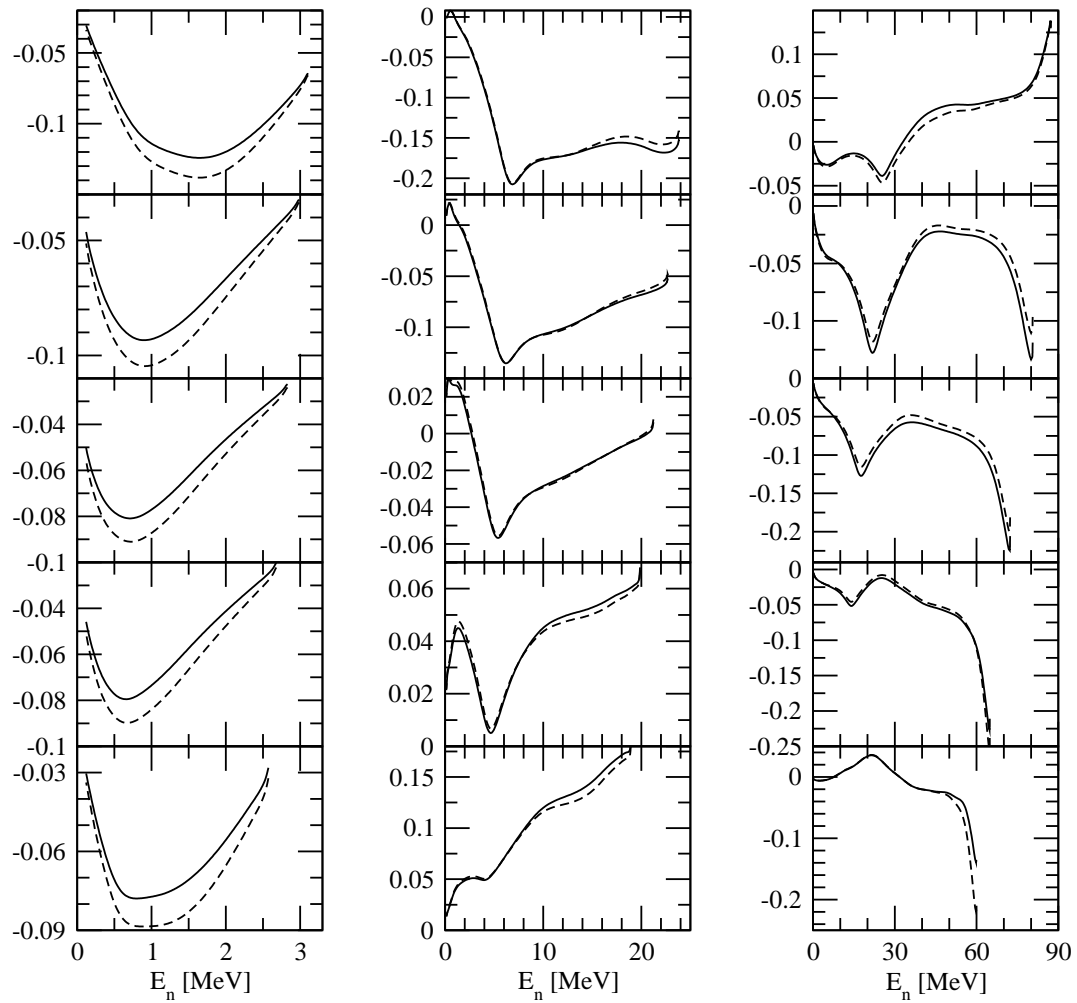


FIG. 8. The same as in Fig. 7 but for the neutron knockout.

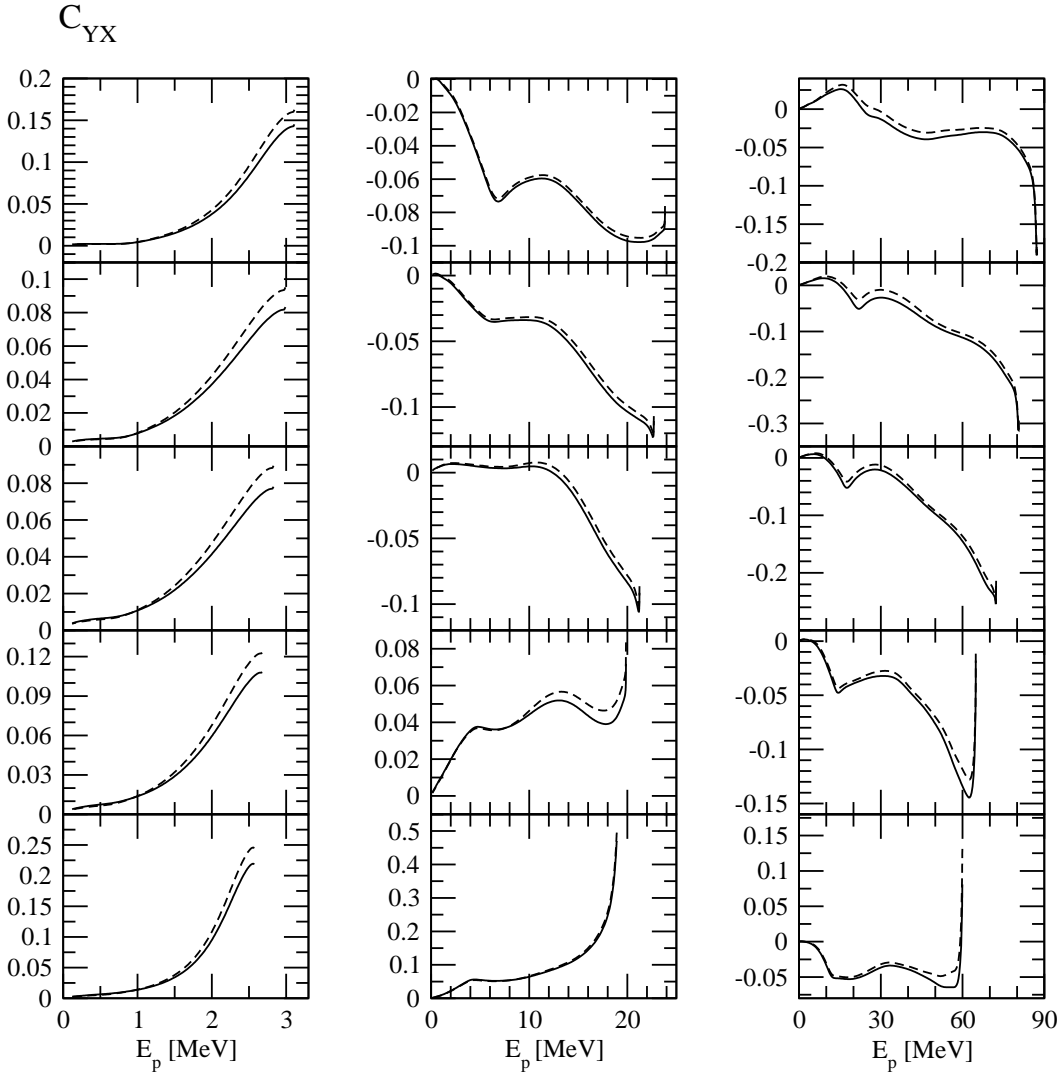


FIG. 9. The spin correlation coefficients $C_{y,x}^{\gamma,{}^3He}(\theta)$ for the proton emission. The photon energies, angles and the curves are as in Fig 1.

C_{YX}

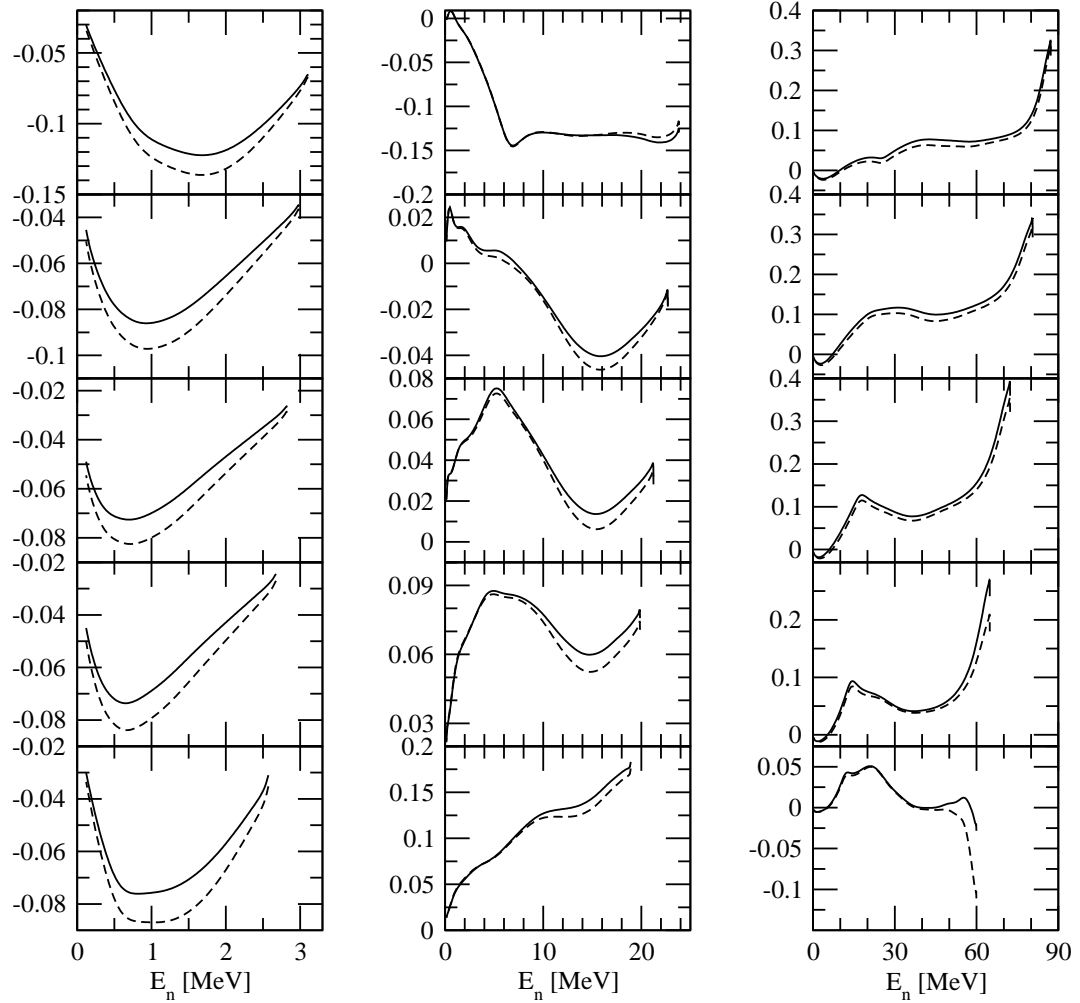


FIG. 10. The same as in Fig. 9 but for the neutron knockout.

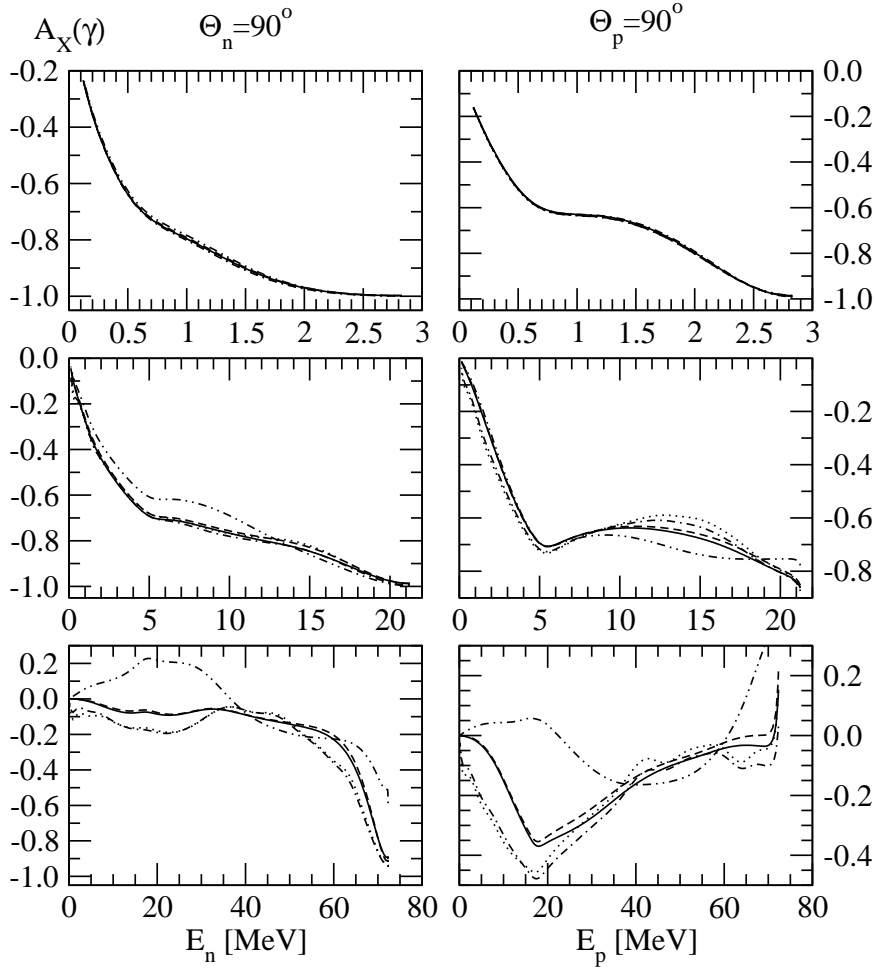


FIG. 11. The photon analyzing power $A_x^\gamma(\theta)$ for the neutron (left column) and the proton (right column) at $E_\gamma = 12$ MeV (the first row), 40 MeV (the second row) and 120 MeV (the third row). The nucleon detection angle is $\theta = 90^\circ$. The double-dot-dashed line corresponds to AV18 predictions with nuclear current taken as single nucleon current only. The dashed (solid) line corresponds to AV18 (AV18+UrbanaIX) predictions based on single nucleon current supplemented by $\pi-$ and $\rho-$ meson exchange currents. The dotted (dash-dotted) line corresponds to AV18 (AV18+UrbanaIX) predictions with many-body contributions to the current taken into account via the Siegert theorem.

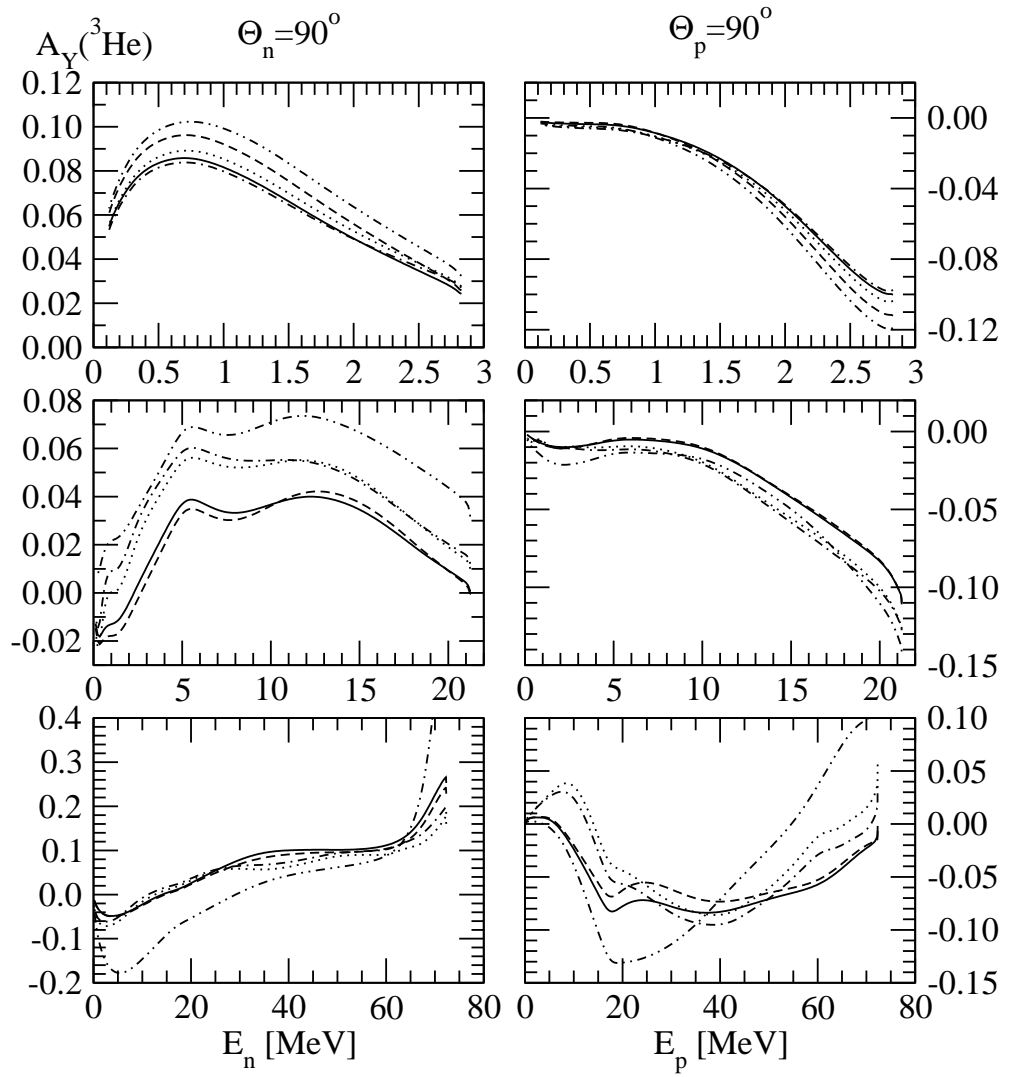


FIG. 12. The same as in Fig. 11 but for the nuclear analyzing power $A_y^{^3He}(\theta)$.

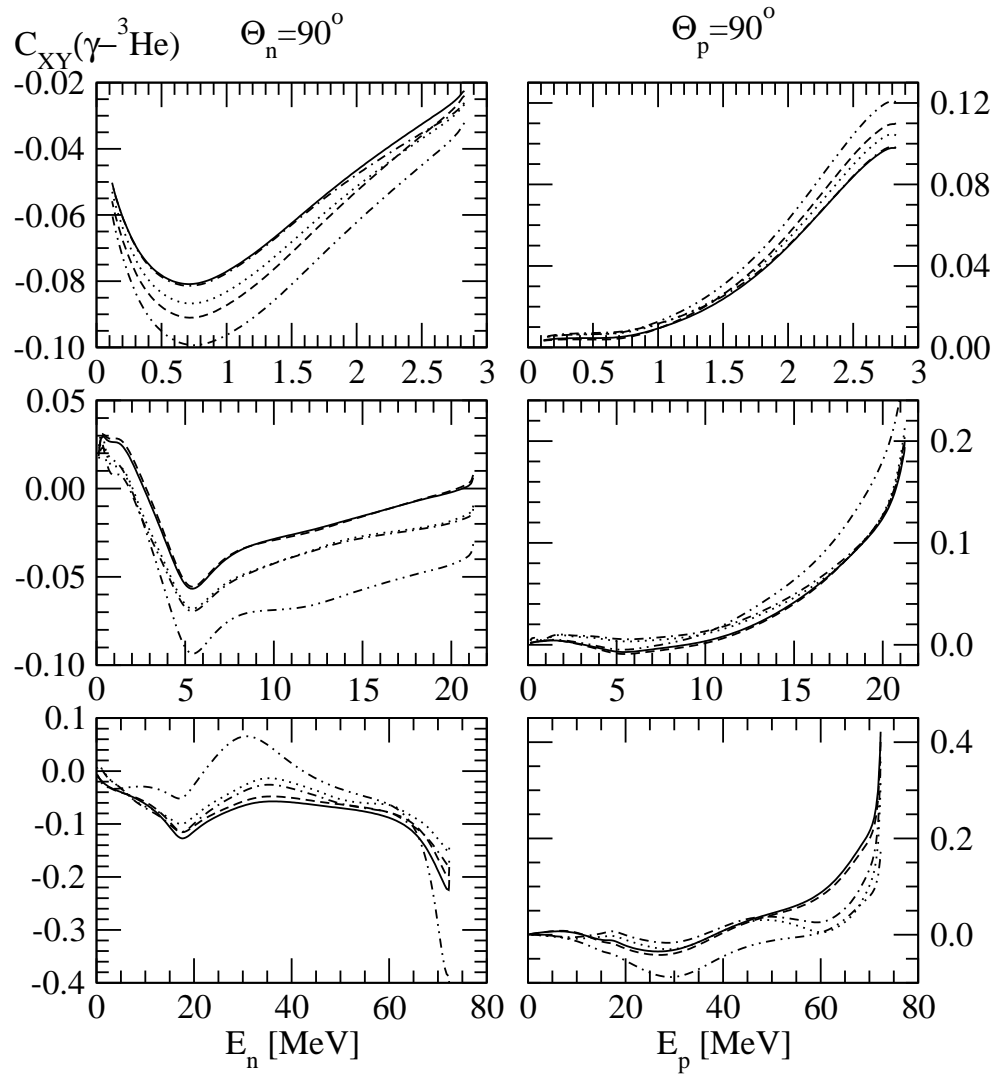


FIG. 13. The same as in Fig. 11 but for the spin correlation coefficients $C_{x,y}^{\gamma, {}^3\text{He}}(\theta)$.

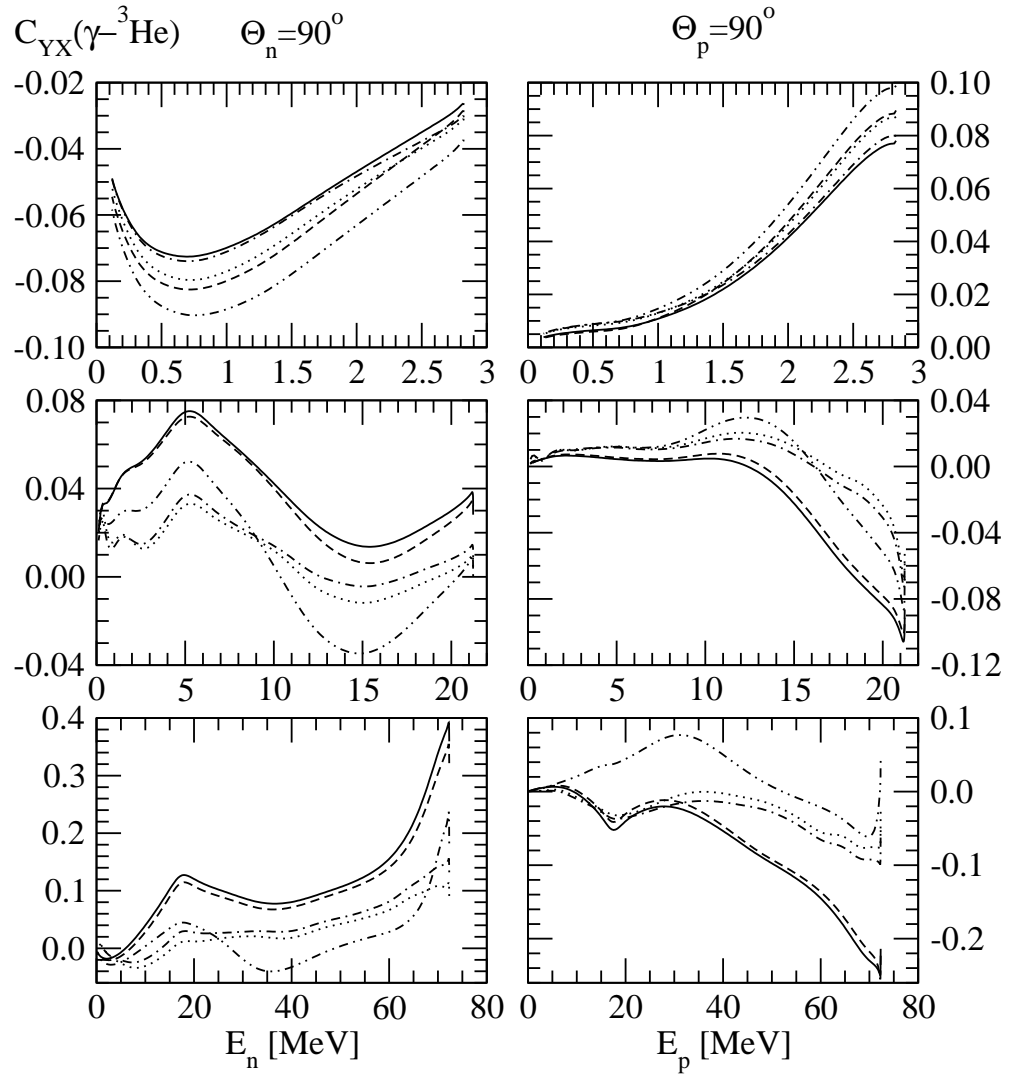


FIG. 14. The same as in Fig. 11 but for the spin correlation coefficients $C_{y,x}^{\gamma, {}^3\text{He}}(\theta)$.

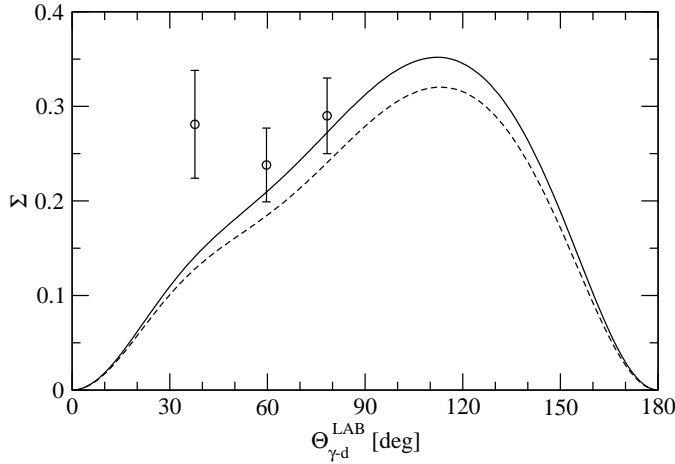


FIG. 15. The cross section asymmetry Σ at $E_\gamma = 120$ MeV. The dashed (solid) curve represents the AV18 (AV18+Urbana IX) predictions. Data are from [25].

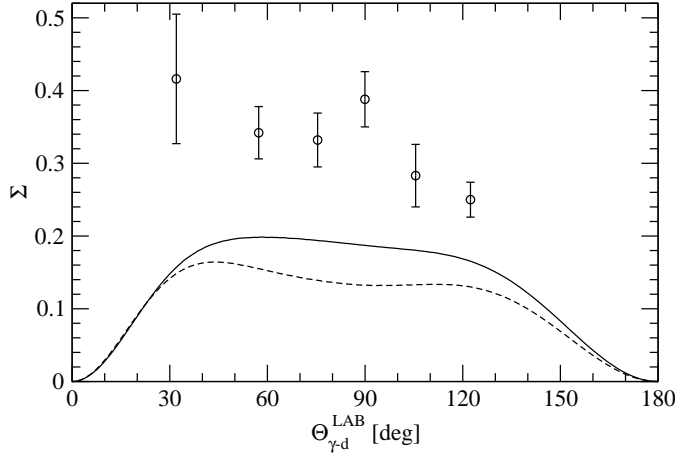


FIG. 16. The cross section asymmetry at $E_\gamma = 200$ MeV. Curves as in Fig. 15 Data are from [25].